J Mater Sci (2011) 46:1655–1667
DOI 10.1007/s10853-010-4983-5

Monoclinic effects and orthotropic estimation for the behaviour of rolled sheet

O. Chahaoui · M. L. Fares · D. Piot · F. Montheillet

Received: 15 June 2010 / Accepted: 5 October 2010 / Published online: 21 October 2010

Abstract The crystallographic texture of an asymmetrically rolled sheet was investigated by electron back scattered diffraction (EBSD) and exhibited prismatic monoclinic symmetry. The parameters of the associated yield equation, derived from the quadratic orthotropic Hill criterion, were determined from the volume fractions of the texture components using the "Continuum Mechanics of Textured Polycrystals" (CMTP) approach. Two quantities are defined to assess the departure from orthotropy, and a method is proposed to find the "best" orthotropic estimation of the sheet behaviour. Results are first discussed on the basis of strain rate ratio predictions. Mechanical behaviour analysis of a sheet submitted to combined shear and compression (CSC) loading is also used to illustrate the method.

List of symbols

RD, TD, ND	Rolling, transverse and normal directions of the sheet
F, G, H, L, M, N	Anisotropy parameters of the Hill orthotropic yield function
F', G', H', L', M', N'	Anisotropy parameters of the Hill orthotropic yield function after a rotation about TD
P, q, r, t	Additional anisotropy parameters associated with monoclinic symmetry
p', q', r', t'	Additional anisotropy parameters associated with monoclinic symmetry after a rotation about TD
$\boldsymbol{M}$	Fourth order tensor associated with a quadratic yield function
$\boldsymbol{M}_0$	Orthotropic part of $\boldsymbol{M}$
$\boldsymbol{M}_{\mathbf{pm}}$	Prismatic monoclinic part of $\boldsymbol{M}$
$R(\theta)$	Strain rate ratio at an angle in the sheet plane
x, y, z	Space coordinates of sheet
x', y', z'	Space coordinates of sheet in the rotated axes about TD
$\dot{\varepsilon}_{ij}$	Strain rate tensor components
θ	Angle between a direction in the sheet plane and the rolling direction RD
τ	Shear stress in the CSC test
σ_{ij}	Stress tensor components
σ_0	Equivalent flow stress
$\sigma = \sigma_{33}$	Normal compression stress in the CSC test
φ_1, Φ, φ_2	Euler angles
ψ	Angle of rotation of the sheet about TD
ψ_0	Value of ψ which minimizes $\|\boldsymbol{M}_{\mathbf{pm}}\|$

O. Chahaoui · D. Piot · F. Montheillet
Centre SMS, CNRS UMR 5146, Ecole Nationale Supérieure des Mines de Saint-Etienne, Saint Etienne, France

O. Chahaoui · M. L. Fares
Metallurgy and Materials Engineering Department, Faculty of Engineering, Badji Mokhtar University, 23000 Annaba, Algeria

M. L. Fares (✉)
Mechanics of Materials and Plant Maintenance Research Laboratory (LR3MI), Metallurgy and Material Engineering Department, Badji Mokhtar University, BP 12, Annaba 23000, Algeria
e-mail: fares.lamine@univ-annaba.org

Introduction

It is a well-known fact that the drawability properties of metal sheet (e.g. occurrence of deep drawing ears, or roping) strongly depend on anisotropy induced by rolling.

This is especially true for aluminium alloys and ferritic steels, which exhibit strong crystallographic textures after hot rolling [1], for two reasons: (i) continuous recrystallization occurs during hot working, which precludes randomization of grain orientations, and (ii) no phase transformation occurs upon cooling. Furthermore, such textures cannot be entirely eliminated or even modified by subsequent cold rolling and/or heat treatments.

There is a vast body of literature concerning the anisotropy/yield surface calculations and also texture gradients resulting from rolling. For instance, in classical (symmetric) rolling, the overall rolled sheet exhibit orthotropic symmetry, although more or less intense shear components of opposite sign may be present close to the rolls [2, 3]. However, the strain rate accompanying rolling deformation is commonly simplified by a plane strain state [4]. Conversely, in asymmetric rolling, where, for instance, the rotation velocities of the cylinders are different [5, 6], the strain rate in the roll gap is rather asymmetrical. Afterwards, the assumption of orthotropic sample symmetry becomes not justified specially in the case of pronounced shear deformation [2]. In this context, Hill [7] assumed conservation of orthotropic symmetry in the study of length change of tube during twisting but this assumption has not been substantiated experimentally. Most of the previous experiments (Bailey et al. [8]; Michino et al. [9]; Stout et al. [10]; Eisenberg et al. [11]; Helling et al. [12]) have been designated to study yield loci in stress spaces without reference to possible orthotropic symmetry and evolution of anisotropy under a plane stress condition for cold-rolled steel sheets. An experimental study conducted by Kim [13] showed that orthotropic symmetry is maintained during twisting of cold drawn tubes and the orientations or orthotropy axes are altered. Darrieulat et al. [14] in earlier work, related to torsion testing (a simple shear deformation), claimed that the Hill yield criterion can be extended to the case of prismatic monoclinic symmetry. According to these earlier quoted assumptions, a potential strong departure from orthotropy is expected and the mechanical behaviour of the sheet is likely to become (prismatic) monoclinic [15, 16]. In that case, the transverse axis TD is a Λ^2 rotation axis (RD, ND) a mirror symmetry plane, but (TD, ND) and (RD, TD) are no longer symmetry planes.

The aim for the present investigative work relates mainly to estimate the effect of the monoclinic parts on the global orthotropic behaviour of a rolled metal sheet in a given symmetry plan. For this purpose, the texture of an asymmetrically rolled metal sheet is characterized in "Texture characterization of the asymmetrically rolled sheet" section. The induced anisotropic behaviour will then be determined using the CMTP approach described in "Monoclinic yield criterion" section for the case of monoclinic symmetry. The orthotropic properties of the sheet are then described in "Orthotropic properties of the sheet" section and the departure from orthotropy is assessed in "Illustration and quantitative assessment of the non-orthotropic sheet behaviour" section. Accordingly, it becomes necessary to define and to estimate the magnitude of a "purely monoclinic" anisotropy component. Finally, in "Discussion: orthotropic estimation of the material behaviour" section, an analysis of the extent to which such sheet can be considered as orthotropic to a first approximation is carried out, and a way to determine the "best" orthotropic estimation of its mechanical behaviour is proposed.

Texture characterization of the asymmetrically rolled sheet

The hot rolled sheet was high purity iron containing 60 ppm C, with a thickness close to 2 mm prior to deformation. In standard rolling, the strain path is essentially plane strain compression plus some shears out mid-plane, leading to more or less locally orthotropic textures. Asymmetric rolling is thus used to intensify the departure from orthotropy of the sheet induced by the intense shear. More specifically, the material was annealed for 45 min at 400 °C and then asymmetrically rolled at room temperature The two cylinders had equal diameters $R = 100$ mm, but quite a large rotation velocity ratio of 15. In order to enforce shears, eight passes (thickness reduction of 20% per pass) were carried out resulting in a final sheet thickness of ~ 0.5 mm.

The plate was cut by spark machining into square specimens of area 10 mm^2. Finally, the asymmetrically rolled plate was subjected to a recrystallization annealing under vacuum at 450 °C for 45 min. To facilitate removing of surface oxides and to avoid surface damage and cutting strain, the sample underwent an electrolytic polishing in a solution containing 950-mL acetic acid and 60-mL perchloric acid at 15 °C under a voltage of 20 V during 10 s.

For microstructure characterizations, that show grain orientation, shape and size, the sample was observed on a plane normal to the transverse direction TD of the sheet. Surface preparation consisted of mechanical grinding by means of P2500 grit-mesh and polishing down to a final step of 1 μm using colloidal silica in suspension. Etching solution was DINO type comprising 140 mL H_2O, 100 mL H_2O_2, 4 g $H_2C_2O_4$, 1.5 mL HF and 2 mL H_2SO_4.

Sample microstructure examinations were carried out by optical microscopy (GX.51 Olympus). Figure 1 shows a cross-section optical micrograph of the cold-rolled material after annealing. The microstructure is very inhomogeneous within which some areas appear fully recrystallized, while

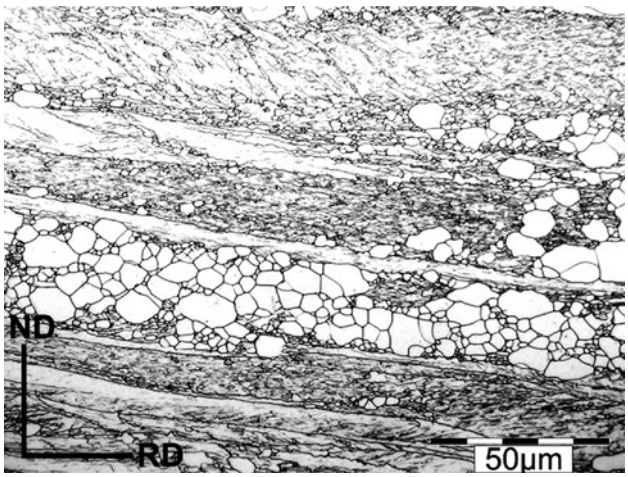

Fig. 1 Cross-section micrograph of asymmetrically rolled and recrystallized as-received sheet

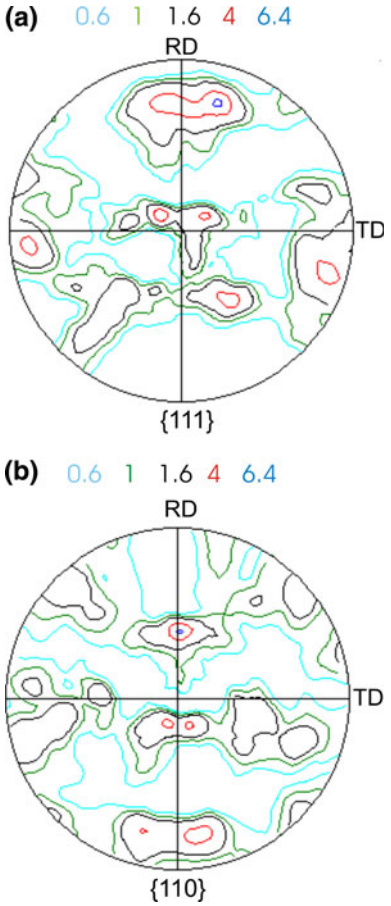

Fig. 2 Pole figures obtained from EBSD measurements on the (RD, ND) plane of the sheet, represented here on the sheet plane: **a** {111} and **b** {110}

others exhibit large shear bands. Texture measurements were achieved using a JSM-6500 F scanning electron microscope equipped with electron back scattered diffraction (EBSD) system. The accelerating voltage was 20 kV. Pole figures accounting for the whole sheet thickness were calculated using *Channel 5* Software (HKL Technology) without any sample symmetry assumptions (triclinic symmetry). As expected, the pole figures display reasonably monoclinic symmetry (symmetry plane normal to TD), as shown in Fig. 2. Among all texture components, both orientations $(323)[\bar{1}\bar{3}3]$ and $[013)[\bar{2}3\bar{1}]$ appear to dominate. Such orientations are not located along the so-called γ *fibre* ($\{111\}\perp$ND) contrarily to conventional rolling of bcc materials [17–19].

From EBSD data and grain reconstruction, an average orientation was computed using *Channel 5* for each grain. A surface fraction, proportional to pixel number, was affected to each reconstructed grain and was identified as usual to the volume fraction. This discrete description of texture was analysed by means of the Van Houtte software (Fast Harmonic Method) [20], representing each orientation by a Gaussian distribution (in orientation space) for spherical harmonics decomposition (assuming monoclinic symmetry). This continuous description allowed redrawing smooth and monoclinic pole figures as shown in Fig. 3.

The discrete description of texture was also analysed in terms of volume fractions of texture components. For the purpose, a limited number of ideal components (listed in Table 1) were considered. Each measured orientation was affected to the "closest" component, in the sense of the minimum misorientations angle. Furthermore, an isotropic (random) component was taken into account [21]. In order to check quantitatively monoclinic symmetry, i.e. symmetry with respect to the (RD, ND) plane, all used orientations and their corresponding Euler angles are listed in Table 1. Such simple, yet quantitative, representation of the data may be compared directly to theoretical predictions and the strain rate ratio $R(\theta)$ can be calculated [22].

Monoclinic yield criterion

The method referred to as Continuum Mechanics of Textured Polycrystals (CMTP) [23–27] allows describing, in a simple way, the anisotropy of textured materials in which one or several ideal orientations are easily identifiable. Reformulated by Darrieulat et al. and extended to the case of prismatic monoclinic symmetry [14, 28], it is based on the quadratic yield equation early proposed by Hill [7, 29]. However, it takes explicitly into account crystallographic texture, which is the primary source of anisotropy. The determination of volume fractions of the various texture components of a rolled sheet exhibiting monoclinic symmetry allows deriving the parameters of the yield equation. Data pertaining to the investigated sheet are reported in Table 1 and will be used in the following. Since several texture components are involved, a homogenization

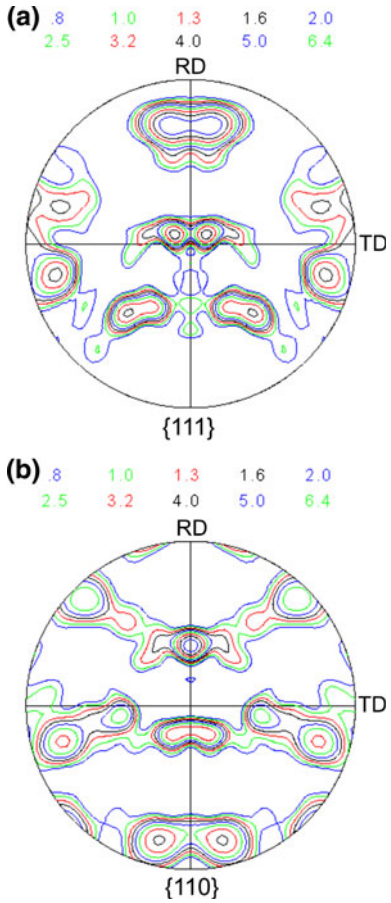

Fig. 3 Reconstructed pole figures after discretization accounting for monoclinic symmetry: **a** {111} and **b** {110}

procedure was carried out using volume fraction weighted averages [14, 28].

For the sake of simplicity, the monoclinic prismatic tensor $\boldsymbol{M}$ will be introduced under the assumptions of uniform stress throughout the material (see details in Appendix 1). Material layers located at various depths in sheet deformed by asymmetric rolling undergo different deformation paths: in particular, surfaces (skins) in contact with rolls are submitted to a simple shear strain rate component, which induces prismatic monoclinic symmetry. Darrieulat and Montheillet [14] have proposed for describing such material anisotropy a homogeneous quadratic polynomial yield equation, insensitive to Bauschinger effect and to hydrostatic pressure (incompressible material) involving nine independent parameters. In the RD, TD and ND sheet axes, it can be written in the form:

$$\begin{aligned} &F(\sigma_{22}-\sigma_{33})^2+G(\sigma_{33}-\sigma_{11})^2+H(\sigma_{11}-\sigma_{22})^2 \\ &\quad+2N\sigma_{12}^2+2M\sigma_{13}^2+2L\sigma_{23}^2+4p\sigma_{12}\sigma_{23} \\ &\quad+4\sigma_{13}(q\sigma_{11}+r\sigma_{22}+t\sigma_{33})=2\sigma_0^2. \end{aligned} \tag{1}$$

Table 1 Volume fractions of the texture components derived from ODF calculations; (1) as measured; (2) corrected for isotropic component

Texture components	Euler angles			Monoclinic (vol.%)			
	φ_1	Φ	φ_2	(1)		(2)	
$(323)[\bar{1}\bar{3}3]$	64	55	60	20.24		18.2	
$(32\bar{3})[\bar{1}\bar{3}\bar{3}]$	−64	125	60	10.90		10.90	
$(013)[\bar{2}3\bar{1}]$	220	20	20	9.90		7.88	
$(01\bar{3})[\bar{2}31]$	140	160	20	5.02		5.00	
$(115)[\bar{5}\bar{5}2]$	90	15	45	0.50		−0.57	
$(11\bar{5})[552]$	90	165	45	3.70		2.70	
$(331)[3\bar{1}\bar{6}]$	290	77	45	2.54	3.80	0.72	0.190
$(33\bar{1})[3\bar{1}6]$	70	102	45	1.26		−0.53	
$(331)[\bar{3}16]$	110	77	45	2.08	2.46	1.720	1.817
$(33\bar{1})[\bar{3}1\bar{6}]$	−110	102	45	0.38		0.097	
$(554)[\bar{2}\bar{2}5]$	90	60	45	3.18		2.23	
$(55\bar{4})[225]$	90	120	45	2.36		1.33	
$(113)[3\bar{1}0]$	0	45	20	3.70	4.56	2.090	1.452
$(133)[\bar{3}10]$	180	45	20	0.86		−0.638	
$(13\bar{3})[\bar{3}10]$	180	135	20	1.32	2.56	0.47	0.970
$(13\bar{3})[3\bar{1}0]$	0	135	20	1.24		0.50	
Random (vol.%)				30.82		47.90	

In which p, q, r and t are monoclinic parameters such as $q+r+t=0$ (insensitivity to hydrostatic pressure). Whenever $p=q=r=t=0$, Eq. 1 reduces to the Hill orthotropic yield equation.

If σ_0^1, σ_0^2 and σ_0^3 are the yield stresses in uniaxial tension along the axes RD, TD and ND, respectively, then:

$$\begin{aligned} &G+H=2\left(\sigma_0/\sigma_0^1\right)^2 \quad F+H=2\left(\sigma_0/\sigma_0^2\right)^2 \\ &F+G=2\left(\sigma_0/\sigma^3\right)^2. \end{aligned} \tag{2}$$

In the same way, if σ_0^{23}, σ_0^{13} and σ_0^{12} are the simple shear stresses along the anisotropy axes:

$$L=\left(\sigma_0/\sigma_0^{23}\right)^2 \quad M=\left(\sigma_0/\sigma_0^{13}\right)^2 \quad N=\left(\sigma_0/\sigma_0^{12}\right)^2. \tag{3}$$

In this section, the yield function (1) will be used in the tensorial form:

$$f(\boldsymbol{\sigma}_{ij})=\boldsymbol{\sigma}:\boldsymbol{M}:\boldsymbol{\sigma}=\boldsymbol{M}_{ijkl}\sigma_{ij}\sigma_{kl}, \tag{4}$$

where the summation is extended over the four indices: i, j, k, $l=1, 2, 3$.

$\boldsymbol{M}$ is a fourth-order tensor exhibiting the same symmetries as the Hooke tensor, i.e. for any values of the indices i, j, k, l:

$$\boldsymbol{M}_{ijkl}=\boldsymbol{M}_{klji}=\boldsymbol{M}_{jikl}=\boldsymbol{M}_{ijlk}. \tag{5}$$

Equation 4 can be written more simply in matrix form as follows:

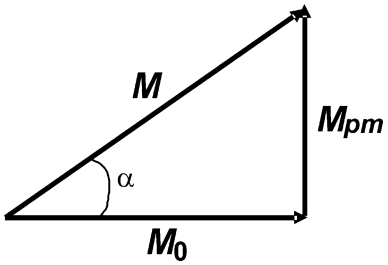

Fig. 4 Schematic illustration of the departure from orthotropic behaviour measured by $\|\boldsymbol{M}_{pm}\|$

$$f(\boldsymbol{\sigma}_{ij}) = \begin{bmatrix} \sigma_{11} \\ \sigma_{22} \\ \sigma_{33} \\ \sqrt{2}\sigma_{23} \\ \sqrt{2}\sigma_{13} \\ \sqrt{2}\sigma_{12} \end{bmatrix}^{T} \begin{bmatrix} G+H & -H & -G & 0 & \sqrt{2}q & 0 \\ -H & F+H & -F & 0 & \sqrt{2}r & 0 \\ -G & -F & F+G & 0 & \sqrt{2}t & 0 \\ 0 & 0 & 0 & L & 0 & p \\ \sqrt{2}q & \sqrt{2}r & \sqrt{2}t & 0 & M & 0 \\ 0 & 0 & 0 & p & 0 & N \end{bmatrix} \times \begin{bmatrix} \sigma_{11} \\ \sigma_{22} \\ \sigma_{33} \\ \sqrt{2}\sigma_{23} \\ \sqrt{2}\sigma_{13} \\ \sqrt{2}\sigma_{12} \end{bmatrix}, \quad (6)$$

where the superscript $\boldsymbol{T}$ denotes the transposed vector.

In any coordinate system, the tensor $\boldsymbol{M}$ can be split into the sum of two tensors as illustrated schematically in Fig. 4:

$$\boldsymbol{M} = \boldsymbol{M}_0 + \boldsymbol{M}_{pm} \quad (7)$$

where $\boldsymbol{M_0}$ can be considered as the projection of $\boldsymbol{M}$ onto the vectorial subspace of tensors associated with an orthotropic behaviour in the considered set of axes.

In matrix representation:

$$\boldsymbol{M}_0 = \begin{bmatrix} G+H & -H & -G & 0 & 0 & 0 \\ -H & F+H & -F & 0 & 0 & 0 \\ -G & -F & F+G & 0 & 0 & 0 \\ 0 & 0 & 0 & L & 0 & 0 \\ 0 & 0 & 0 & 0 & M & 0 \\ 0 & 0 & 0 & 0 & 0 & N \end{bmatrix} \quad (8)$$

$\boldsymbol{M_{pm}}$ is in turn associated with "purely monoclinic" behaviour:

$$\boldsymbol{M}_{pm} = \begin{bmatrix} 0 & 0 & 0 & 0 & \sqrt{2}q & 0 \\ 0 & 0 & 0 & 0 & \sqrt{2}r & 0 \\ 0 & 0 & 0 & 0 & \sqrt{2}t & 0 \\ 0 & 0 & 0 & 0 & 0 & p \\ \sqrt{2}q & \sqrt{2}r & \sqrt{2}t & 0 & 0 & 0 \\ 0 & 0 & 0 & p & 0 & 0 \end{bmatrix} \quad (9)$$

The above parameters have been quantitatively introduced into the macroscopic formulation of the CMTP approach. For that purpose, a numerical parametric investigation was performed, leading to the derivation of the parameters for the individual components and the overall sheet (Table 2).

Orthotropic properties of the sheet

It is interesting to note that whenever $\sigma_{23} = \sigma_{13} = 0$, Eq. 1 reduces to the classical Hill orthotropic yield criterion. This means practically that any mechanical test involving stresses confined in the sheet plane is unable to reveal a departure from orthotropic behaviour. For instance, the usual strain rate ratio $R(\theta)$ can be predicted from the F, G, H, L, M and N orthotropy parameters (measured from mechanical tests or derived from the texture components), without using the complete yield equation (1). Figure 5a shows $R(\theta)$ for the investigated sheet obtained from data reported in Table 2 and Fig. 5b illustrates the influence of each individual texture component on R for $\theta = 0$.

Table 2 Anisotropy parameters for the individual texture components and the overall sheet in the coordinate system (RD, TD and ND)

	$(323)[\bar{1}\bar{3}3]$	$(013)[\bar{2}3\bar{1}]$	$(115)[\bar{5}\bar{5}2]$	$(331)[3\bar{1}\bar{6}]$	$(554)[\bar{2}\bar{2}5]$	$(113)[3\bar{1}0]$	Overall sheet
F	0.1378	0.3029	0.3114	0.0943	0.1094	0.0651	0.2528
G	0.1551	0.2573	0.2725	0.2481	0.1705	0.2773	0.2615
H	0.1873	0.1138	0.0597	0.2124	0.2617	0.2829	0.2505
L	0.8000	0.4697	0.4527	0.8869	0.8567	0.9453	0.8531
M	0.7653	0.5609	0.5306	0.5794	0.7346	0.5209	0.8356
N	0.7010	0.8480	0.9562	0.6508	0.5522	0.5097	0.8576
p	−0.3037	0.1370	−0.3095	0.0378	0.5065	−0.1949	−0.0691
q	0.0516	0.1210	−0.0851	−0.0848	−0.2279	0.1455	0.0372
r	0.1073	0.0484	−0.1094	0.0133	0.1790	−0.0689	−0.0244
t	0.0557	−0.1695	0.1945	0.0714	0.0488	−0.0765	−0.0128

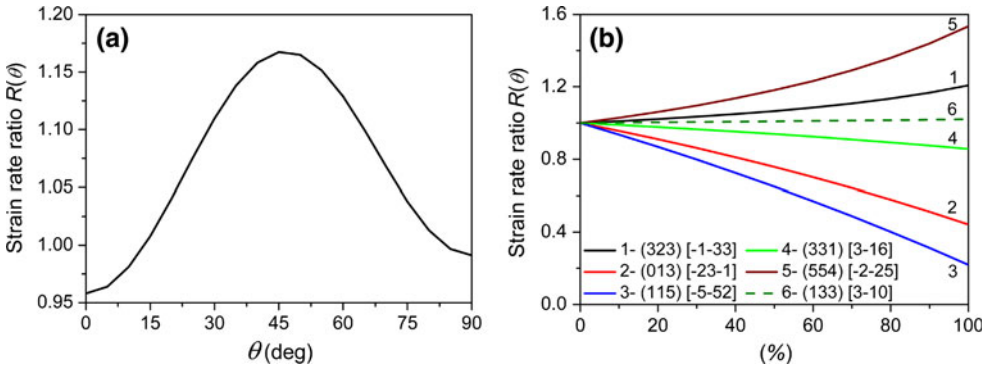

Fig. 5 The strain rate ratio $R(0)$in the sheet plane showing the angular dependence in **a** and volume fractions dependence of the various texture components in **b**

Illustration and quantitative assessment of the non-orthotropic sheet behaviour

As shown in the previous section, conventional mechanical tests (e.g. tensile test or strain rate ratio measurements) are not appropriate to characterize the mechanical behaviour of sheet exhibiting prismatic monoclinic symmetry, such as imposed by the boundary conditions of the asymmetric rolling process. As a consequence, the departure from orthotropy cannot be easily assessed. For this purpose, a simple test of combined shear and compression (CSC) can be proposed, in which the prescribed stress state is quite similar to the case of asymmetric rolling. The normal compression stress $\sigma_{zz} = \sigma$ and shear stress $\sigma_{xz} = \tau$ are imposed along the specimen axes x, y and z as shown in Fig. 6. The expression of the stress tensor in the sample reference frame ($\boldsymbol{S}$) is:

$$\boldsymbol{\sigma_S} = \begin{bmatrix} 0 & 0 & \tau \\ 0 & 0 & 0 \\ \tau & 0 & \sigma \end{bmatrix}. \tag{10}$$

Using the rotation matrix $\boldsymbol{P}$ from the specimen ($\boldsymbol{S}$) to the sheet ($\boldsymbol{R}$) axes leads to the expression of the stress tensor in the latter reference frame:

$$\boldsymbol{\sigma_R} = \boldsymbol{P}\sigma_S\boldsymbol{P}^T. \tag{11}$$

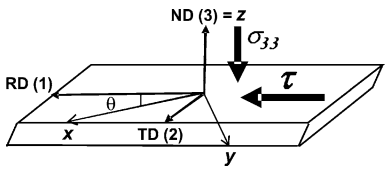

Fig. 6 Geometry of the combined shear and compression test (CSC)

Using the boundary conditions prescribed in the combined shear-compression test, the quadratic yield function (1) leads to a second degree polynomial equation; the unique positive root is (Appendix 2):

The monoclinic behaviour of the sheet can be estimated by

$$\tau = \frac{-2t\sigma\cos\theta + \left(4t^2\sigma^2\cos^2\theta - [2L\sin^2\theta + 2M\cos^2\theta][(F+G)\sigma^2 - 2\sigma_0^2]\right)^{1/2}}{2L\sin^2\theta + 2M\cos^2\theta}. \tag{12}$$

the difference in shear stress τ along the two opposite directions θ and $\theta + \pi$:

$$\tau(\theta+\pi) - \tau(\theta) = \frac{2t\sigma\cos\theta}{L\sin^2\theta + M\cos^2\theta}. \tag{13}$$

In particular, for $\theta = 0$ (rolling direction):

$$\Delta\tau = \tau(\pi) - 2t\sigma/M. \tag{14}$$

From which the parameter t could be in principle measured.

Figure 7a shows the normalized shear stress $\tau(\theta)/\tau(\theta)$ dependence on the angle θ between the shear direction and the rolling direction for a compression stress $\sigma = \sigma_0$. In Fig. 7b, the dependence of $\tau(\theta)/\tau(\theta)$ on the compression stress σ/σ_0 is illustrated for various angles θ ranging from 0° to 315°. Finally, the components of the associate strain rate tensor are given in Fig. 8. Anisotropy parameters listed in Table 2 were used for these three diagrams. It can be seen that for a given value of σ, the maximum value of the shear stress τ is attained along the rolling direction ($\theta = 0°$). Table 3 shows the contribution of each monoclinic texture component. It appears that the component $(115)[\bar{5}\bar{5}2]$ has a strong monoclinic effect despite its small volume fraction in the material. However, it is very asymmetric with respect to the transverse axis (TD).

In a more general way, the departure from orthotropy can be estimated by the norm of tensor $\boldsymbol{M_{pm}}$ defined by Eq. 9:

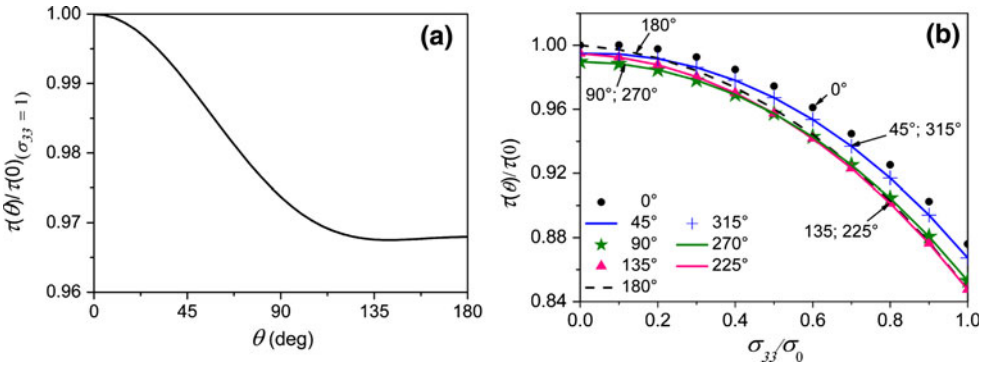

Fig. 7 The normalized shear stress in the CSC test showing the angular dependence for a normal compression stress with $\sigma = \sigma_0$ in **a** and the normalized compression stress σ_{33}/σ_0 dependence for various orientations in the sheet plane in **b**

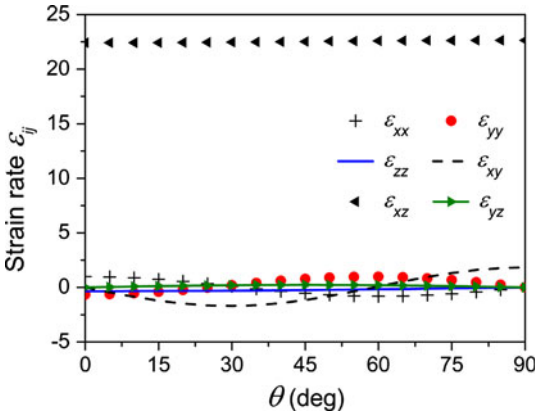

Fig. 8 Angular dependence of the strain rate components where θ is the angle between the shear direction of the CSC test and the rolling direction

Table 3 Assessment of the departure from orthotropic behaviour in the coordinate system (RD, TD and ND)

Orientations	δ	$\|\Delta\tau\|$	$\delta\cdot\|\Delta\tau\|$	$\|\|\boldsymbol{M}_{pm}\|\|$	$\|\|\boldsymbol{M}_{0}\|\|$	α (°)
(323)[$\bar{1}\bar{3}$3]	7.30	0.145	1.058	0.503	1.477	18.80
(013)[$\bar{2}3\bar{1}$]	2.88	0.604	1.740	0.469	1.490	17.48
(115)[$\bar{5}\bar{5}$2]	3.27	0.733	2.400	0.648	1.529	22.96
(331)[$3\bar{1}\bar{6}$]	1.62	0.246	0.400	0.229	1.483	08.80
(554)[$\bar{2}\bar{2}$5]	0.90	0.133	0.120	0.926	1.483	32.00
(113)[$3\bar{1}$0]	0.48	0.294	0.141	0.450	1.516	16.55
Overall sheet	–	0.0307	–	0.1348	1.825	4.22

$$\left\|\boldsymbol{M}'_{pm}\right\| = \left(2p^2 + 4(q^2 + r^2 + t^2)\right)^{1/2}. \tag{15}$$

Or by the angle α between $\boldsymbol{M_0}$ and $\boldsymbol{M}$, as shown schematically in Fig. 4, with:

$$\tan\alpha = \frac{\|\boldsymbol{M}_{pm}\|}{\boldsymbol{M_0}} = \left(\frac{2p^2 + 4(q^2 + r^2 + t^2)}{(G+H)^2 + (F+H)^2 + (G+F)^2 + 2F_2 + 2G^2 + 2H^2 + L^2 + M^2 + N^2}\right)^{1/2}. \tag{16}$$

Table 3 illustrates the departure from orthotropy for the various individual texture components, as well as for the overall texture of the sheet, estimated through $\Delta\tau$, $\|\boldsymbol{M}_{pm}\|$ and α. In the second column of the table, δ denotes the fraction of monoclinic contribution associated with each non-orthotropic texture component, while the product $\delta\Delta\tau$ in column 4 estimates the effective contribution of the component. It appears that the (115) [$\bar{5}\bar{5}$2] component has a strong effect on the overall anisotropy, despite its low volume fraction in the material. It is worth to note, however, that the overall ($\alpha \approx 4.22°$) remains weak, although the intense shear prescribed during asymmetric rolling was likely to promote monoclinic symmetry.

Discussion: orthotropic estimation of the material behaviour

In a coordinate system (RD′, TD, ND′) rotated about the symmetry axis TD by an angle ψ, the yield equation (1) takes a new form, still corresponding to monoclinic symmetry. In each of these reference frames, the departure from orthotropy can be measured by the norm $\|\boldsymbol{M}'_{pm}\|$. It is quite natural to look for the angle ψ corresponding to the minimum value of $\|\boldsymbol{M}_{pm}\|$, thus providing the "best" orthotropic estimation of the sheet behaviour. For that purpose, it is first necessary to use a set of independent variables, i.e. the deviatoric stress components s_{11}, s_{22}, s_{23}, s_{13} and s_{12}. The monoclinic plasticity criterion (1) then takes the form:

$$\begin{aligned}&(F+4G+H)s_{11}^2 + (4F+G+H)s_{22}^2\\ &\quad + (4F+4G-2H)s_{11}s_{22} + 2Ls_{23}^2 + 2Ms_{13}^2 + 2Ns_{12}^2\\ &\quad + 4ps_{12}s_{23} + 4s_{13}[(2q+r)s_{11} + (q+2r)s_{22})] = 2\sigma_0^2.\end{aligned} \tag{17}$$

In which only nine independent parameters F, G, H, L, M, N, p, q, and r are involved since $q + r + t = 0$. Using the rotation matrix, the stress components s_{ij} are expressed in terms of their counterparts s_{ij}' in the rotated frame and substituted into Eq. 17. This gives a new polynomial in the variables s_{ij}', which must be identified with the canonical form:

$$\begin{aligned}&(F' + 4G' + H')s_{11}^2 + (4F' + G' + H')s_{22}^2 + (4F' + 4G' \\ &\quad - 2H')s_{11}s_{22} + 2L's_{23}^2 + 2M's_{13}^2 + 2N's_{12}^2 + 4p's_{12}s_{23} \\ &\quad + 4s_{13}[(2q' + r')s_{11} + (q' + 2r')s_{22}] \\ &\quad = 2\sigma_0^2\end{aligned} \tag{17'}$$

This leads to a system of nine linear equations for the nine unknowns F', G', H', L', M', N', p', q' and r':

$$\begin{aligned}F' &= \frac{1}{2}(F + H) + \frac{1}{2}(F - H)\cos 2\psi + r\sin 2\psi \\ G' &= \frac{1}{8}(4G - F - H + 2M) \\ &\quad + \frac{1}{8}(4G + F + H - 2M)\cos 4\psi + \frac{1}{2}(q - t)\sin 4\psi \\ H' &= \frac{1}{2}(F + H) - \frac{1}{2}(F - H)\cos 2\psi - r\sin 2\psi \\ L' &= \frac{1}{2}(L + N) + \frac{1}{2}(L - N)\cos 2\psi - p\sin 2\psi \\ M' &= \frac{1}{4}(4G + F + H + 2M) \\ &\quad - \frac{1}{4}(4G + F + H - 2M)\cos 4\psi - (q - t)\sin 4\psi \\ N' &= \frac{1}{2}(L + N) - \frac{1}{2}(L - N)\cos 2\psi + p\sin 2\psi \\ p' &= \frac{1}{2}(L - N)\sin 2\psi + p\cos 2\psi \\ q' &= -\frac{1}{8}(4G + F + H - 2M)\sin 4\psi + \frac{1}{4}(F - H)\sin 2\psi \\ &\quad + \frac{1}{2}(q - t)\cos 4\psi + \frac{1}{2}(q + t)\cos 2\psi \\ r' &= \frac{1}{2}(H - F)\sin 2\psi + r\cos 2\psi\end{aligned} \tag{18}$$

The dependence of the norm $\|\boldsymbol{M}_{pm}'\|$ on angle ψ is depicted in Fig. 9 for the various individual texture components and the overall texture of the sheet, respectively. For the latter, the minimum is obtained for $\psi \approx 35°$. This angle defines a reference frame in which the mechanical behaviour of the sheet is the closest to an orthotropic behaviour. While in the original sheet axis $\|\boldsymbol{M}_{pm}'\| \approx 0.13$, it drops to ≈ 0.11 in the rotated frame. The corresponding anisotropy coefficients are listed in Table 4, and the parameters used for estimating the departure from orthotropy are given in Table 5.

In the new reference frame rotated by the angle $\psi = 35°$ about the transverse direction (Fig. 10), the departure from orthotropy is still significant, but clearly much less than in the initial sheet plane. In Fig. 11, the departure from orthotropic behaviour in the sheet plane is measured by $|\Delta\tau(\theta)|$ associated with a CSC test, as defined in Eq. 14 above. The equivalent parameter $|\Delta\tau'(\theta)|$ in the rotated plane is also plotted in the figure, which shows that the material behaviour is much closer to orthotropy in the new reference axes.

The orthotropy parameters of the "best" orthotropic estimation of the sheet behaviour can be used for deriving a new orthotropic strain rate ratio $R(\theta)$. Figure 12 shows that the latter slightly differs from the original $R(\theta)$ function. This means that the "best" orthotropic estimation of the overall sheet behaviour may not be the best orthotropic estimation of a given specific property, like the strain rate ratio which remains orthotropic in nature in any reference system.

In addition, it is interesting to note that if the minimum value of $\|\boldsymbol{M}_{pm}\|$ is zero, it means that the sheet monoclinic symmetry is only apparent, whereas its effective symmetry is orthotropic. The necessary condition for an apparently monoclinic sheet to be orthotropic in some reference frame rotated by an angle ψ with respect to the initial axes is $\|\boldsymbol{M}_{pm}'\| = 0$ which is tantamount to $p' = q' = r' = 0$. This leads to two conditions relating the initial monoclinic parameters and to the derivation of the angle ψ (Appendix 3).

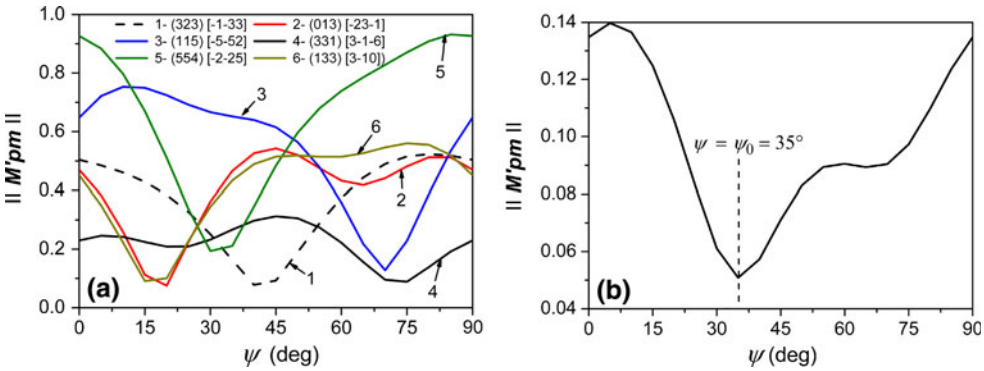

Fig. 9 Angular dependence of the norm $\|\boldsymbol{M}_{pm}'\|$ used to measure the departure from orthotropy of the prismatic monoclinic equation (ψ is the rotation angle about the transverse direction TD) for various texture components in **a** and for the overall sheet texture in **b**

Table 4 Anisotropy parameters for the individual texture components and the overall sheet in a coordinate system (RD′, TD and ND′) rotated about the symmetry axis TD by an angle ψ

	$(323)[\bar{1}\bar{3}3]$	$(013)[\bar{2}3\bar{1}]$	$(115)[\bar{5}\bar{5}2]$	$(331)[3\bar{1}\bar{6}]$	$(554)[\bar{2}\bar{2}5]$	$(113)[3\bar{1}0]$	Overall sheet
F'	0.0532	0.2862	0.1257	0.1458	−0.0087	0.0720	0.2290
G'	0.2829	0.2791	0.0943	0.1669	0.3513	0.2570	0.3045
H'	0.2719	0.1305	0.2453	0.1610	0.3799	0.2760	0.2742
L'	1.0528	0.4654	0.9092	0.7736	1.2326	0.9852	0.9196
M'	0.5097	0.5173	0.8870	0.7418	0.3730	0.5616	0.7496
N'	0.4481	0.8523	0.4997	0.7641	0.1764	0.4698	0.7912
p'	−0.0573	−0.1308	−0.3424	0.1238	−0.0302	0.1379	−0.0257
q'	0.0320	−0.0123	0.2711	−0.0369	−0.1492	−0.2601	−0.0036
r'	−0.0367	0.0165	−0.0374	0.0045	−0.0612	−0.0235	−0.0083
t'	−0.0650	0.2623	0.1211	−0.1340	−0.0040	−0.0232	0.0151

Table 5 Assessment of the departure from orthotropic behaviour in the reference axes rotated by $\psi = 35°$

Orientations	δ	$\|\Delta\tau'\|$	$\delta \cdot \|\Delta\tau'\|$	$\|\boldsymbol{M}_{pm}'\|$	$\|\boldsymbol{M}_{\mathbf{0}}'\|$	α' (°)
$(323)[\bar{1}\bar{3}3]$	7.30	0.046	0.335	0.484	1.474	18.18
$(013)[\bar{2}3\bar{1}]$	2.88	0.208	0.600	0.333	1.454	12.90
$(115)[\bar{5}\bar{5}2]$	3.27	0.286	0.935	0.383	1.479	22.56
$(331)[3\bar{1}\bar{6}]$	1.62	0.172	0.278	0.117	1.472	4.552
$(554)[\bar{2}\bar{2}5]$	0.90	0.020	0.018	0.864	1.505	29.85
$(113)[3\bar{1}0]$	0.48	0.082	0.040	0.419	1.462	15.99
Overall sheet	–	0.017	–	0.111	1.826	3.50

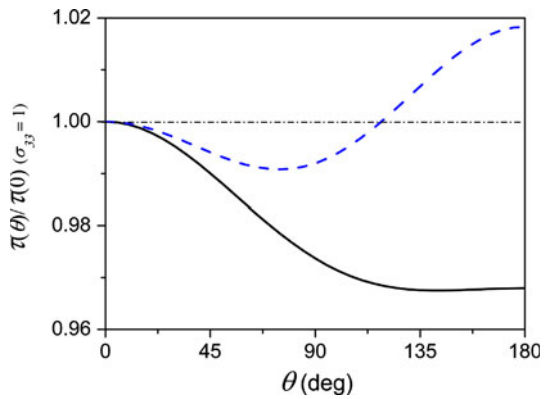

Fig. 10 Angular dependence of the normalized CSC shear stress in the plane rotated by the angle $\psi = 35°$ about TD (*broken line*). The *solid line* shows the initial shear stress angular dependence in the sheet plane

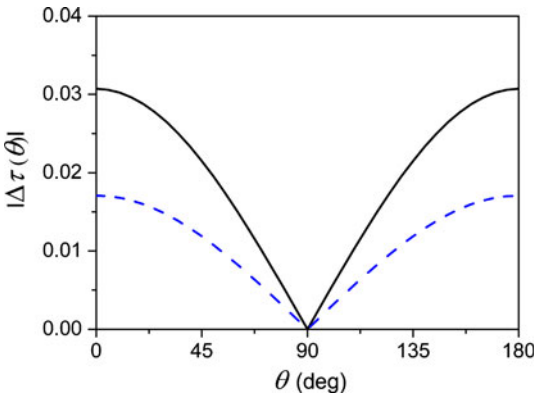

Fig. 11 Angular dependence of the monoclinic effect measured by $|\Delta\tau(\theta)|$, where θ is the angle between the shear direction of the CSC test and the rolling direction (*solid line*). The equivalent monoclinic effect $|\Delta\tau'(\theta)|$ in the plane rotated by an angle $\psi = 35°$ about TD is shown by the *broken line*

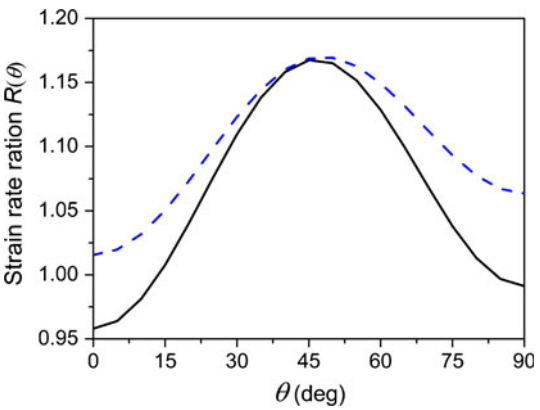

Fig. 12 Angular dependence of the strain rate ratio $R(\theta)$, where θ is the angle between the tensile and rolling directions (*solid line*). The *broken line* shows the new strain rate ratio obtained from the "best" orthotropic estimation of the sheet behaviour

Conclusions

The mechanical behaviour of an asymmetrically rolled sheet was investigated using a monoclinic yield equation derived from the quadratic Hill orthotropic yield criterion. The associated anisotropy parameters were determined from the volume fractions of the various texture components using the CMTP method. The main results are the following:

1. The departure of the sheet from orthotropy, although quite low, is significant. It can be quantitatively estimated by a scalar parameter $\|\boldsymbol{M}'_{\boldsymbol{pm}}\|$.
2. The "purely monoclinic" component of anisotropy has no effect on any mechanical test in which stresses are exerted within the sheet plane. In particular, the strain rate ratio $R(\theta)$ is insensitive to non-orthotropic effects.
3. A combined shear-compression (CSC) test was proposed to bring into evidence such non-orthotropic effects.
4. Since departure from orthotropy is limited, it was suggested that the mechanical behaviour of such sheet can be considered to a first estimation as orthotropic. The "best" choice of the orthotropy axes can then be derived by minimization of $\|\boldsymbol{M}_{\boldsymbol{pm}}\|$.

Acknowledgements This work was financially supported by CNRS/DPGRF Cooperation Program, no. SPI 18446 and by PNE program from Algerian Ministry of Higher Education and Scientific Research (MESRS).

Appendix 1

The CMTP method

The mechanical behaviour of the texture components can be associated with a quadratic yield criterion [27, 29]:

$$f(\boldsymbol{\sigma}_{ij}) = \boldsymbol{\sigma} : \boldsymbol{M} : \boldsymbol{\sigma} = \boldsymbol{M}_{ijkl}\sigma_{ij}\sigma_{kl}, \tag{1.1}$$

with

$$[\boldsymbol{M}] = A[\boldsymbol{U}] + (1-A)[\boldsymbol{V}], \tag{1.2}$$

where $\boldsymbol{M}$, $\boldsymbol{U}$ and $\boldsymbol{V}$ are three-dimensional fourth rank tensors defined in the axes of each ideal component. $\mathbf{U}$ is the unit tensor defined in the orthotropy reference frame by $\boldsymbol{U}_{ijkl} = (1/2)(\delta_{ik}\delta_{jl} + \delta_{il}\delta_{jk})$. When $A = 1$, $[\boldsymbol{M}] = [\boldsymbol{U}]$ (isotropic case).

The tensor $\boldsymbol{V}$ is defined in the $\langle 100\rangle$ axes of each texture component: $\boldsymbol{V}_{ijkl} = 1$ if $i = j = k = l$ and $\boldsymbol{V}_{ijkl} = 0$ otherwise. The transformation matrix $\boldsymbol{q}$ from the crystal ($\boldsymbol{C}$) to the specimen ($\boldsymbol{S}$) reference frame can be written in the form:

$$[\boldsymbol{q}] = \begin{bmatrix} q_{11} & q_{12} & q_{13} \\ q_{21} & q_{22} & q_{23} \\ q_{31} & q_{32} & q_{33} \end{bmatrix} = \begin{bmatrix} u_1 & u_2 & u_3 \\ v_1 & v_2 & v_3 \\ w_1 & w_2 & w_3 \end{bmatrix} = \begin{bmatrix} \frac{u}{\sqrt{p_1}} & \frac{v}{\sqrt{p_1}} & \frac{w}{\sqrt{p_1}} \\ \frac{kw-lv}{\sqrt{p_1 p_2}} & \frac{lu-hw}{\sqrt{p_1 p_2}} & \frac{hv-ku}{\sqrt{p_1 p_2}} \\ \frac{h}{\sqrt{p_2}} & \frac{k}{\sqrt{p_2}} & \frac{l}{\sqrt{p_2}} \end{bmatrix}, \tag{1.3}$$

with $p_1 = u^2 + v^2 + w^2$ and $p_2 = h^2 + k^2 + l^2$.

The rule of tensor transformations takes the simple form

$$[\boldsymbol{V}^i]_S = \boldsymbol{V}_{mnrs} = \sum_{t=1}^{3} q_{mt}q_{nt}q_{rt}q_{st} = q_{m1}q_{n1}q_{r1}q_{s1} + q_{m2}q_{n2}q_{r2}q_{s2} + q_{m3}q_{n3}q_{r3}q_{s3} \tag{1.4a}$$

or

$$[\boldsymbol{V}^i]_S = \begin{bmatrix} V_{1111} & V_{1122} & V_{1133} & \sqrt{2}V_{1112} & \sqrt{2}V_{1113} & \sqrt{2}V_{1123} \\ V_{1122} & V_{2222} & V_{2233} & \sqrt{2}V_{2212} & \sqrt{2}V_{2213} & \sqrt{2}V_{2223} \\ V_{1133} & V_{2233} & V_{3333} & \sqrt{2}V_{3312} & \sqrt{2}V_{3313} & \sqrt{2}V_{3323} \\ \sqrt{2}V_{1112} & \sqrt{2}V_{2212} & \sqrt{2}V_{3312} & 2V_{1212} & 2V_{1213} & 2V_{1223} \\ \sqrt{2}V_{1113} & \sqrt{2}V_{2213} & \sqrt{2}V_{3313} & 2V_{1213} & 2V_{1313} & 2V_{1323} \\ \sqrt{2}V_{1123} & \sqrt{2}V_{2223} & \sqrt{2}V_{3323} & 2V_{1223} & 2V_{1323} & 2V_{2323} \end{bmatrix}. \tag{1.4b}$$

The prismatic monoclinic tensor of the symmetrized texture components of the rolled sheet is given as follows:

$$[\boldsymbol{V}^i]_S = \begin{bmatrix} V_{1111} & V_{1122} & V_{1133} & 0 & \sqrt{2}V_{1113} & 0 \\ V_{1122} & V_{2222} & V_{2233} & 0 & \sqrt{2}V_{2213} & 0 \\ V_{1133} & V_{2233} & V_{3333} & 0 & \sqrt{2}V_{3313} & 0 \\ 0 & 0 & 0 & 2V_{1212} & 0 & 2V_{1223} \\ \sqrt{2}V_{1113} & \sqrt{2}V_{2213} & \sqrt{2}V_{3313} & 0 & 2V_{1313} & 0 \\ 0 & 0 & 0 & 2V_{1223} & 0 & 2V_{2323} \end{bmatrix}. \tag{1.4c}$$

Using the homogeneous function when several texture components are present and taking the average for several common orientations of volume fractions f_i then gives:

$$[\boldsymbol{V}] = \sum_{i=1}^{N} f_i[\boldsymbol{V}^i] \quad \text{and} \quad f_0 = 1 - \sum_{i=1}^{N} f_i, \tag{1.5}$$

where f_0 is the volume fraction of the random part of the texture.

In the same way, for the symmetric tensor of the plasticity criterion $[\boldsymbol{M}] = \sum_{i=0}^{N} f_i[\boldsymbol{M}_i]$, this under the assumptions of uniform stress can be written:

$$[\boldsymbol{M}] = \sum_{i=0}^{N} f_i[\boldsymbol{M}_i] \quad (i = 0, 1\ldots, N) \tag{1.6}$$

$$[\boldsymbol{M}] = f_0[\boldsymbol{M}_0] + f_1[\boldsymbol{M}_1] + f_2[\boldsymbol{M}_2] + \cdots + f_N[\boldsymbol{M}_N] \tag{1.7}$$

$$[\boldsymbol{M}] = f_0[\boldsymbol{U}] + A[\boldsymbol{U}](f_1 + f_2 + \cdots + f_N) + (1-A)(f_1[\boldsymbol{V}^1] + f_2[\boldsymbol{V}^2] + \cdots + f_N[\boldsymbol{V}^N]) \tag{1.8}$$

with

$$f_0 + f_1 + f_2 + \cdots + f_N = 1 \quad \text{and} \quad [\boldsymbol{V}] = \sum_{i=1}^{N} f_i [\boldsymbol{V}^i].$$

Thus,

$$[\boldsymbol{M}] = f_0[\boldsymbol{U}] + A[\boldsymbol{U}](1 - f_0) + (1 - A)[\boldsymbol{V}]. \tag{1.8a}$$

Equation 1.8a, leads to the monoclinic prismatic yield function as it follows:

$$2\sigma_0^2 = \boldsymbol{\sigma}^T [\boldsymbol{M}] \boldsymbol{\sigma}.$$

Or

$$2\bar{\sigma}_0^2 = \begin{bmatrix} \sigma_{11} \\ \sigma_{22} \\ \sigma_{33} \\ \sqrt{2}\sigma_{23} \\ \sqrt{2}\sigma_{13} \\ \sqrt{2}\sigma_{12} \end{bmatrix}^T \begin{bmatrix} M_{1111} & M_{1122} & M_{1133} & 0 & M_{1113} & 0 \\ M_{1122} & M_{2222} & M_{2233} & 0 & M_{2213} & 0 \\ M_{1133} & M_{2233} & M_{3333} & 0 & M_{3313} & 0 \\ 0 & 0 & 0 & M_{2323} & 0 & M_{2312} \\ M_{1113} & M_{2213} & M_{3313} & 0 & M_{1313} & 0 \\ 0 & 0 & 0 & M_{1223} & 0 & M_{2323} \end{bmatrix} \begin{bmatrix} \sigma_{11} \\ \sigma_{22} \\ \sigma_{33} \\ \sqrt{2}\sigma_{23} \\ \sqrt{2}\sigma_{13} \\ \sqrt{2}\sigma_{12} \end{bmatrix}. \tag{1.9}$$

Using the following properties:

$$2\sigma_{11}\sigma_{22} = \sigma_{33}^2 - \sigma_{11}^2 - \sigma_{22}^2$$

$$2\sigma_{11}\sigma_{33} = \sigma_{22}^2 - \sigma_{33}^2 - \sigma_{11}^2$$

$$2\sigma_{22}\sigma_{33} = \sigma_{11}^2 - \sigma_{22}^2 - \sigma_{33}^2$$

The expansion of Eq. 1.9 gives:

$$\begin{aligned} 2\bar{\sigma}_0^2 = {} & A\sigma_{11}^2 + B\sigma_{22}^2 + C\sigma_{33}^2 + 2M_{1212}\sigma_{12}^2 + 2M_{1313}\sigma_{13}^2 \\ & + 2M_{2323}\sigma_{23}^2 + 8M_{1223}\sigma_{12}\sigma_{23} + 4\sigma_{13}(M_{1113}\sigma_{11} \\ & + M_{2213}\sigma_{22} + M_{3313}\sigma_{33}) \end{aligned} \tag{1.10}$$

where

$$A = M_{1111} - M_{1122} - M_{1133} + M_{2233} \tag{1.10a}$$

$$B = M_{2222} - M_{1122} + M_{1133} - M_{2233} \tag{1.10b}$$

$$C = M_{3333} + M_{1122} - M_{1133} - M_{2233} \tag{1.10c}$$

By analogy with the Hill prismatic monoclinic criterion, the above equation can finally be written:

$$\begin{aligned} 2\bar{\sigma}_0^2 = {} & (2H + 2G - F)\sigma_{11}^2 + (2F + 2H - G)\sigma_{22}^2 + (2F \\ & + 2G - H)\sigma_{33}^2 + 2L\sigma_{12}^2 + 2M\sigma_{13}^2 + 2N\sigma_{23}^2 \\ & + 4p\sigma_{12}\sigma_{23} + 4\sigma_{13}(q\sigma_{11} + r\sigma_{22} + t\sigma_{33}) \end{aligned} \tag{1.11}$$

Appendix 2

The combined shear-compression (CSC) test

The stress tensor can be written in the specimen (***S***) axes in the form:

$$\boldsymbol{\sigma_S} = \begin{bmatrix} 0 & 0 & \tau \\ 0 & 0 & 0 \\ \tau & 0 & \sigma \end{bmatrix}, \tag{2.1}$$

where $\tau = \sigma_{xz}$ the shear is stress and σ is the compression stress.

Using the rotation of the matrix ***P*** about (ND//Z), from the specimen (***S***) to the sheet axes (***R***) and the transposed matrix $\boldsymbol{P^T}$ (Fig. 6):

$$\boldsymbol{P} = \begin{bmatrix} \cos\theta & -\sin\theta & 0 \\ \sin\theta & \cos\theta & 0 \\ 0 & 0 & 1 \end{bmatrix} \quad \boldsymbol{P^T} = \begin{bmatrix} \cos\theta & \sin\theta & 0 \\ -\sin\theta & \cos\theta & 0 \\ 0 & 0 & 1 \end{bmatrix} \tag{2.2}$$

The stress tensor in the new reference axes (***R***) can be written:

$$\begin{aligned} \boldsymbol{\sigma_R} &= \boldsymbol{P}\,\boldsymbol{\sigma_S}\,\boldsymbol{P^T} \\ &= \begin{bmatrix} \cos\theta & -\sin\theta & 0 \\ \sin\sigma & \cos\theta & 0 \\ 0 & 0 & 1 \end{bmatrix} \begin{bmatrix} 0 & 0 & \tau \\ 0 & 0 & 0 \\ \tau & 0 & \sigma \end{bmatrix} \begin{bmatrix} \cos\theta & \sin\theta & 0 \\ -\sin\theta & \cos\theta & 0 \\ 0 & 0 & 1 \end{bmatrix} \end{aligned}$$

$$\boldsymbol{\sigma_S} = \begin{bmatrix} 0 & 0 & \tau\cos\theta \\ 0 & 0 & \tau\sin\theta \\ \tau\cos\theta & \tau\sin\theta & \sigma \end{bmatrix} \tag{2.3}$$

Afterwards, the monoclinic criterion gives:

$$\begin{aligned} & (2L\sin^2\theta + 2M\cos^2\theta)\tau^2 + 4t\cos\theta\sigma\tau + (F + G)\sigma^2 \\ & \quad = 2\sigma_0^2. \end{aligned} \tag{2.4}$$

The positive root of this second degree polynomial equation is

$$\tau = \frac{-2t\sigma\cos\theta + \left(4t^2\sigma^2\cos^2\theta - [2L\sin^2\theta + 2M\cos^2\theta][(F + G)\sigma^2 - 2\sigma_0^2]\right)^{1/2}}{2L\sin^2\theta + 2M\cos^2\theta} \tag{2.5}$$

$$\text{For } \theta = 0, \quad \tau_1 = \frac{-2t\sigma + \left(4t^2\sigma^2 - 2M[(F+G)\sigma^2 - 2\sigma_0^2]\right)^{1/2}}{2M},$$
$$\text{For } \theta = \pi, \quad \tau_1 = \frac{2t\sigma + \left(4t^2\sigma^2 - 2M[(F+G)\sigma^2 - 2\sigma_0^2]\right)^{1/2}}{2M}. \tag{2.6}$$

The monoclinic effect is the difference between the positive and negative shear directions in the sheet plane:

$$\Delta\tau = \tau_2 - \tau_1 = \frac{2t\sigma}{M}. \tag{2.7}$$

More generally,

$$\tau(\theta + \pi) - \tau(\theta) = \frac{2t\sigma\cos\theta}{L\sin^2\theta + M\cos^2\theta}. \tag{2.8}$$

Application of the normality rule to the monoclinic prismatic yield equation then gives the strain rate tensor:

$$\dot{\varepsilon}_{ij} = \dot{\lambda}\frac{\partial f(\sigma_{ij})}{\partial\sigma_{ij}} \quad \dot{\lambda} \geq 0 \tag{2.9}$$

wherefrom:

$$\dot{\varepsilon}_{xx} = 2\dot{\lambda}\{-(F\sin^2\theta + G\cos^2\theta)\sigma + [(p+r)\sin 2\theta\sin\theta + 2q\cos^3\theta]\tau\}$$
$$\dot{\varepsilon}_{yy} = 2\dot{\lambda}\{-(F\cos^2\theta + G\sin^2\theta)\sigma + [(q-p)\sin 2\theta\sin\theta + 2r\cos^3\theta]\tau\}$$
$$\dot{\varepsilon}_{xy} = 2\dot{\lambda}\{(G-F)\sigma\sin 2\theta + [(2r-2q)\sin 2\theta\cos\theta + 2p\cos 2\theta\sin\theta]\tau\}$$
$$\dot{\varepsilon}_{xz} = 2\dot{\lambda}[2t\cos\theta\sigma + 2(M\cos^2\vartheta + L\sin^2\theta)\tau]$$
$$\dot{\varepsilon}_{yz} = 2\dot{\lambda}[-2t\sin\theta\sigma + [L-M]\sin 2\theta\tau]$$
$$\dot{\varepsilon}_{zz} = -(\dot{\varepsilon}_{xx} + \dot{\varepsilon}_{yy})$$

Appendix 3

Apparently monoclinic behaviour

The apparently monoclinic material is in fact orthotropy if and only if the following three equations are simultaneously fulfilled:

$$p' = \frac{1}{2}(L-N)\sin 2\psi + p\cos 2\psi = 0$$
$$q' = -\frac{1}{8}(4G + F + H - 2M)\sin 4\psi + \frac{1}{4}(F-H)\sin 2\psi + \frac{1}{2}(q-t)\cos 4\psi + \frac{1}{2}(q+t)\cos 2\psi = 0 \tag{3.1}$$
$$r' = \frac{1}{2}(H-F)\sin 2\psi + r\cos 2\psi = 0$$

Combination of the first and third equations gives immediately

$$\tan 2\psi = \frac{2p}{N-L} \tag{3.2}$$

and

$$\frac{p}{N-L} = \frac{r}{F-H}. \tag{3.3}$$

Substitution of Eq. 3.3 into the second equation of Eq. 3.1 then leads to:

$$\frac{q-t}{F+4G+H-2M} = \frac{p(N-L)}{(N-L)^2 - 4p^2} \tag{3.4}$$

It can therefore be concluded that the sheet is orthotropic if both Eqs. 3.3 and 3.4 are fulfilled while the angle ψ defining the orthotropic axes is then given by Eq. 3.2.

References

1. Tóth LS (2009) Microstructure and texture in steels, Part III:225
2. Engler O, Huh MY, Tome CN (2000) Metall Mater Trans A31:2299
3. Sidor J, Miroux A, Petrov R, Kestens L (2008) Acta Mater 56:2495
4. Kim JK, Jee YK, Huh MY, Jeong HT (2004) J Mater Sci 39:5365. doi:10.1023/B:JMSC.0000039246.72708.0a
5. Roumina R, Sinclair CW (2008) Metall Mater Trans 39:2495
6. Watanabe H, Mukai T, Ishikaw K (2004) J Mater Sci 39:1477. doi:10.1023/B:JMSC.0000013922.16079.d3
7. Hill R (1950) The mathematical theory of plasticity. Oxford University Press, Oxford
8. Bailey JA, Haas SL, Nawab KC (1971) J Basic Eng Trans ASME, Paper No. 71-Met-Y
9. Michino MJ Jr, Flindey WN (1974) J Eng Mater Technol Trans ASME 96:56
10. Stout MG, Hecker SS, Boursier R (1983) J Eng Mater Technol Trans ASME 105:242
11. Eisenberg MA, Yen CF (1984) J Eng Mater Technol Trans ASME 106:355
12. Helling DE, Miller AK, Stout MG (1987) J Eng Mater Techol Trans ASME 108:313
13. Kim KH (1992) J Mech Phys Solids 40:127
14. Darrieulat M, Montheillet F (1996) Int J Mech Sci 38:1273
15. Wauthier A, Réglé H, Formigoni J, Herman G (2009) Mater Character 60:90
16. Huh MY, Lee KR, Engler O (2004) Int J Plast 20:1183
17. Lee AU, Kang ED, Kobayashi T (2003) In: 3rd International symposium on designing processing and properties of advanced engineering materials, South Korea, p 6
18. Lee AU, Lee DN (2001) Int J Mech Sci 43:1997
19. Sakai T, Yoneme T, Yoneda K, Saito Y (2003) In: 4th International conference on processing and manufacturing of advanced materials. University of Carlos III, Madrid, Spain, pp 426–424
20. Van Houtte P (1995) The MTM-FHM Software System, Version 2, users manual. Katholieke Universiteit, Leuven, Belgium
21. Chahaoui O (2010) Modélisation mécanique de l'anisotropie d'une tôle présentant un gradient de texture dans son épaisseur. PhD Thesis, Université d'Annaba, Algeria
22. De Paepe A, Herman JC, Leroy V (1997) Steel Res Int 68:479

23. Montheillet F, Gilormini P, Jonas JJ (1985) Acta Metall 33:705
24. Lequeu P (1986) Crystallographic and continuum yield surfaces for textured polycrystals. PhD Thesis, McGill University, Montréal
25. Lequeu P, Montheillet F, Jonas JJ (1985) Textures in non ferrous metals and alloys. AIME Symp Detroit, p 189
26. Lequeu P, Gilormini P, Montheillet F, Bacroix B, Jonas JJ (1987) Acta Metall 35:1159
27. Darrieulat M, Montheillet F (2003) Int J Plast 19:517
28. Darrieulat M (1993) Prévision du comportement plastique anisotrope des polycristaux texturés par la mécanique des milieux continus. PhD Thesis, Ecoles des Mines de Saint-Étienne et de Paris, France
29. Hill R (1948) Proc R Soc Lond A193:281